IRAQI JOURNAL OF MATERIALS
Volume (4) Issue (3) July-September 2025, pp. 125-130

Low-Pressure Pulsed-Laser Deposition of ZnMgO Nanostructures from Sputtered Zn-Coated Mg Target

Ayad J. Faraj, Kamel O. Salman

Department of Physics, College of Science, University of Misan, Al-Amarah, IRAQ

Abstract
In this work, zinc-doped magnesium oxide nanostructures were synthesized by pulsed-laser deposition technique at low pressure. A zinc-coated magnesium target was prepared by magnetron sputtering technique to be irradiated by Nd:YAG laser pulses in presence of oxygen inside deposition chamber. Nanostructured zinc-doped magnesium oxide thin films were deposited on glass substrates. Two main parameters were studied; laser pulse energy and thickness of zinc layer on magnesium target, which was determined by sputtering time. As the film thickness was minimized (~50nm), the structural characterization showed that only ZnMgO structures were found in the final sample. As well, using higher energy of laser pulse has caused the nanoparticle size to be smaller.

Keywords: Pulsed-laser deposition; ZnMgO; Nanostructures; Sputtering
Received: 20 April 2025; **Revised:** 10 June 2025; **Accepted:** 17 June 2025; **Published:** 1 July 2025

1. Introduction

Zinc magnesium oxide (ZnMgO) nanostructures are ternary oxide semiconductors formed by alloying ZnO with MgO. ZnO is a well-known wide-bandgap semiconductor with a bandgap of about 3.37 eV, while MgO has an even wider bandgap (about 7.8 eV) [1-4]. The incorporation of magnesium into the ZnO lattice increases the bandgap tunability, making ZnMgO nanostructures valuable for optoelectronic applications. The bandgap of $Zn_{1-x}Mg_xO$ can be engineered between 3.37 eV and approximately 4.3 eV depending on the Mg content, enabling ultraviolet (UV) photodetection and emission tuning [5-8]. Physically, ZnMgO nanostructures can take various morphologies, including nanorods, nanowires, nanoparticles, and thin films. These nanostructures exhibit high crystallinity and optical transparency in the visible region, along with strong UV absorption [9,10]. The wurtzite structure of ZnO can be retained up to a certain Mg content (typically $x < 0.4$); higher Mg concentrations can induce phase separation or formation of the cubic MgO phase [11]. ZnMgO is stable under ambient conditions and shows improved resistance to corrosion and oxidation compared to pure ZnO. The material is chemically inert in many solvents, but it can be etched under specific acidic or basic environments. The addition of Mg can suppress native defects like oxygen vacancies in ZnO, thereby enhancing the electrical and optical properties of the nanostructure [12-15].

ZnMgO nanostructures are synthesized using various physical and chemical methods. Common preparation techniques include sol-gel method. This solution-based technique offers excellent control over composition and homogeneity. It involves the hydrolysis and condensation of zinc and magnesium precursors followed by drying and annealing [16,17]. ZnMgO nanostructures are also synthesized by hydrothermal method, which is conducted at moderate temperatures and pressures, hydrothermal methods are widely used for fabricating ZnMgO nanorods or nanowires with controlled dimensions [18,19]. ZnMgO nanostructures are also synthesized by chemical vapor deposition (CVD) techniques those are employed for high-quality thin film growth, offering superior crystallinity and surface uniformity [20,21]. Pulsed-laser deposition (PLD) can also be used to synthesize ZnMgO nanostructures. This technique enables precise stoichiometric transfer from target to substrate and is suitable for creating ZnMgO thin films with tunable Mg content [22,23]. These nanostructures can be synthesized by both RF and DC sputtering methods, which are commonly used for depositing ZnMgO films. Co-sputtering from ZnO and MgO targets allows precise control over the Mg content [24,25].

ZnMgO nanostructures find diverse applications owing to their tunable bandgap and enhanced chemical stability. In UV photodetectors, with a wide and adjustable bandgap, ZnMgO is ideal for solar-blind and UV-A/B detectors with high sensitivity and fast response times [26-28]. In light-emitting diodes (LEDs), ZnMgO-based heterostructures are promising candidates for short-wavelength LED applications due to efficient electron-hole recombination [29,30]. In solar cells as a window layer or

buffer layer in thin-film solar cells, ZnMgO improves light harvesting and electrical conductivity [31,32]. In gas sensors, the enhanced surface area and stability of ZnMgO nanoparticles make them suitable for detecting gases such as NO_2, ethanol, and H_2 at low concentrations. ZnMgO films serve as transparent conducting oxide (TCO) layers in display panels and photovoltaic devices due to their transparency and electrical conductivity [33,34].

In this work, zinc-doped magnesium oxide nanostructures were synthesized by pulsed-laser deposition technique at low pressure. A zinc-coated magnesium target was prepared by magnetron sputtering technique to be irradiated by Nd:YAG laser pulses in presence of oxygen inside deposition chamber. Nanostructured zinc-doped magnesium oxide thin films were deposited on glass substrates.

2. Experimental Part

The experimental part of this work includes two main parts; deposition of zinc films on magnesium substrates by sputtering of highly-pure zinc target with argon discharge plasma inside vacuum chamber. The vacuum chamber is made of stainless steel with inside diameter of 50 cm and height of 50 cm. This chamber was evacuated down to 10^{-5} torr using diffusion pump and filled with highly-pure argon gas at pressures ranging in 0.01-0.08 torr. Discharge voltage of 3.5 kV was applied between cathode and anode to generate plasma at discharge current of 35 mA. The Zn target was placed on the cathode while the Mg substrate was mounted on the anode. Both were 5 cm in diameter and 0.3 mm in thickness. The inter-electrode distance was optimized at 5 cm and the deposition time was controlled in order to control the thickness of the grown film.

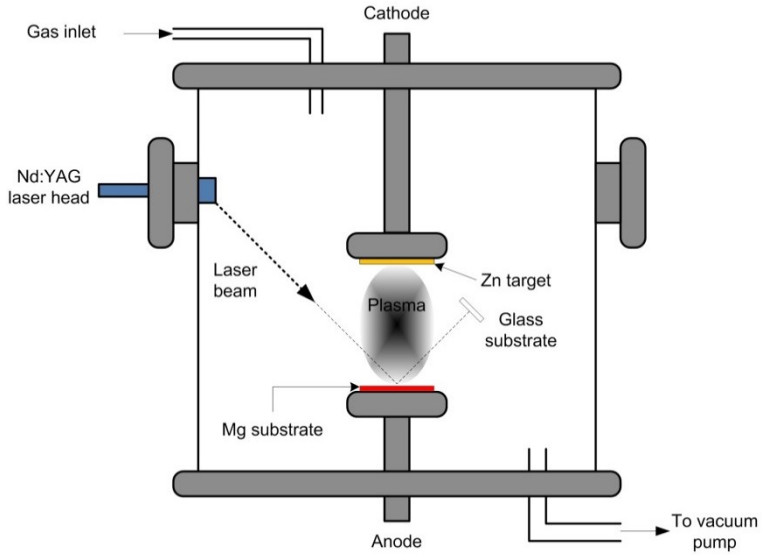

Fig. (1) Experimental setup of this work

After completion of Zn film deposition, the Mg substrate was irradiated with pulses from a 1.064 μm Nd:YAG laser at different pulse energies. The ablated particles were deposited on glass substrate placed at 4 cm from the Zn-coated Mg substrate. The films thickness was measured by laser interferometer method using 630 nm diode laser and the required optics.

Optical measurements were carried out by a SpectraAcademy UV-Visible spectrophotometer within the range of 166-962 nm with accuracy of ~2.0 nm full width at half maximum (FWHM). The structures of the prepared samples were introduced by the x-ray diffraction (XRD) patterns using Bruker X-Ray Diffractometer, 1.54.5Å CuKα radiation in the range 20-70 degrees. The particle size was determined by TESCAN Vega EasyProbe scanning electron microscope (SEM) while the topography of the prepared surfaces was introduced by atomic force microscopy (AFM) using Angstrom AA3000 SPM. The formation of molecular bonds was determined by Fourier-transform infrared (FTIR) microscopy using Shimadzu FTIR-8400S instrument.

3. Results and Discussion

Figure (2) shows a linear correlation between sputtering time and film thickness and he black dashed line represents a best-fit linear regression, confirming a uniform deposition rate throughout the process. This uniform trend is indicative of a highly controlled and stable sputtering environment, which is

essential for reproducible thin film properties. From these data, the Zn thickness increases from 22 nm at 15 min to 200 nm at 120 min. Therefore, the average deposition rate is about 1.70 nm/min. This matches the slope inferred from the regression line in this chart and confirms the consistent deposition throughout the sputtering session, as well as no visible saturation, target poisoning, or re-sputtering effects over time [35].

This linearity has major implications for the growth of ZnMgO via pulsed laser deposition (PLD) using Zn interlayers. Thickness directly influences crystallinity, grain size, and alloying behavior. In ZnMgO nanostructures, at low Zn thickness (e.g., < 50 nm), Mg diffusion may dominate, leading to weaker ZnMgO peaks and more disorder. At moderate thickness (~150 nm), Zn content is sufficient for forming well-defined ZnMgO alloy peaks, as seen in XRD. Beyond 200 nm, there may be phase separation, with MgO segregating due to limited solubility in the ZnO matrix. This plot can be used to predict sputtering times needed for desired thicknesses, to ensure reproducibility of device-grade thin films (e.g., UV photodetectors, TCOs, LEDs), to serve as a calibration curve for thin film manufacturing, and to support the optimization of multilayer and gradient alloy films [36,37]

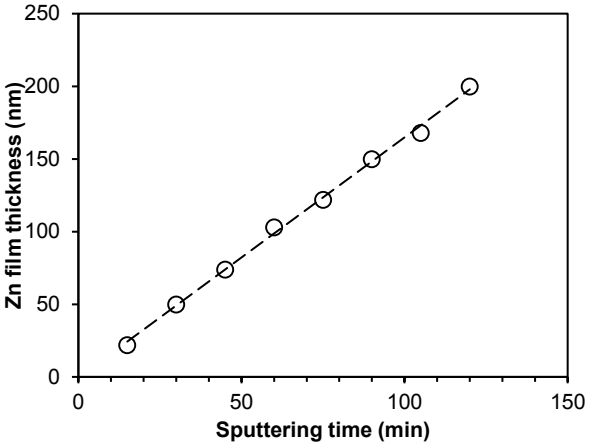

Fig. (2) Variation of Zn film thickness with sputtering time

The X-ray diffraction (XRD) patterns shown in Fig. (3) represent ZnMgO nanostructures synthesized using PLD technique, with varying Zn layer thicknesses of 50 nm, 150 nm, and 200 nm. The analysis focuses on phase formation, crystallinity, phase separation, and strain evolution in relation to layer thickness and the XRD patterns cover the 2θ range from 20° to 70°. Multiple peaks corresponding to ZnO, MgO, and ZnMgO phases are clearly identified. With increasing Zn layer thickness, the intensity of the peaks increases, indicating enhanced crystallinity and grain growth. The peaks are sharp and well-defined, suggesting that the materials are highly crystalline. Major diffraction peaks assigned to ZnO are present at approximately 2θ ≈ 31.8°, 34.4°, 36.3°, 47.5°, 56.6°, 62.8°, and 68°, corresponding to the (100), (002), (101), (102), (110), (103), and (112) planes respectively (based on JCPDS card No. 36-1451). The consistent presence of ZnO peaks across all thicknesses confirms that ZnO retains its wurtzite structure after Mg incorporation. Peaks attributed to MgO appear around 2θ ≈ 42.9° and 62.3°, corresponding to the (200) and (220) planes of cubic MgO (JCPDS card No. 45-0946). The presence of distinct MgO peaks at all thicknesses indicates partial phase separation of MgO, meaning not all magnesium is fully incorporated into the ZnO lattice. Peaks labeled ZnMgO (e.g., at ~34.9° and 60.2°) suggest the formation of a solid solution or alloy phase. These peaks appear between the ZnO and MgO peak positions, which is expected because ZnMgO is a substitutional alloy. The slight shift in the ZnMgO peak positions compared to pure ZnO indicates lattice distortion due to the substitution of smaller Mg^{2+} ions for Zn^{2+} ions [38].

Lower peak intensities suggest limited crystallite growth and lower crystallinity. Peaks are broader, indicating smaller grain size and/or higher microstrain. The ZnMgO peak is less pronounced, implying lower alloying efficiency or incomplete diffusion of Mg into ZnO. Sharp increase in peak intensity and narrowing of peaks imply better crystallinity, larger grain size, and reduced defects. ZnMgO peaks become more distinct, indicating a higher degree of solid solution formation. Phase separation is still evident, but the ZnMgO phase is more dominant than in the 50 nm sample. Highest intensities and sharpest peaks indicate superior crystal quality. ZnMgO peaks are strongest here, confirming effective Mg incorporation at thicker Zn layers. However, the clear presence of MgO peaks alongside suggests

 ISSN (print) 2958-8960 (online) 3006-6042 Printed in IRAQ

solubility limit has been approached or exceeded, leading to Mg-rich phase segregation [39]. Using the Scherrer equation:

$$D = \frac{K\lambda}{\beta cos\theta} \quad (1)$$

The broadening of peaks at thinner Zn layers (50 nm) implies smaller crystallite size and/or higher strain. Peak sharpening at 150 and 200 nm confirms grain coarsening and relaxation of strain during growth.

Zn layer thickness strongly affects the crystallinity, grain size, and phase composition of ZnMgO films. At lower thickness (50 nm), Mg incorporation is limited and leads to weak ZnMgO signals. Optimal alloying occurs at intermediate thickness (150 nm), where the ZnMgO phase dominates with minimal phase separation. At high thickness (200 nm), although crystallinity improves further, phase separation becomes more pronounced, possibly due to the limited solubility of Mg in ZnO lattice. The results indicate that tuning the Zn layer thickness is a key parameter for optimizing phase purity and optical/electrical properties of ZnMgO thin films grown by PLD.

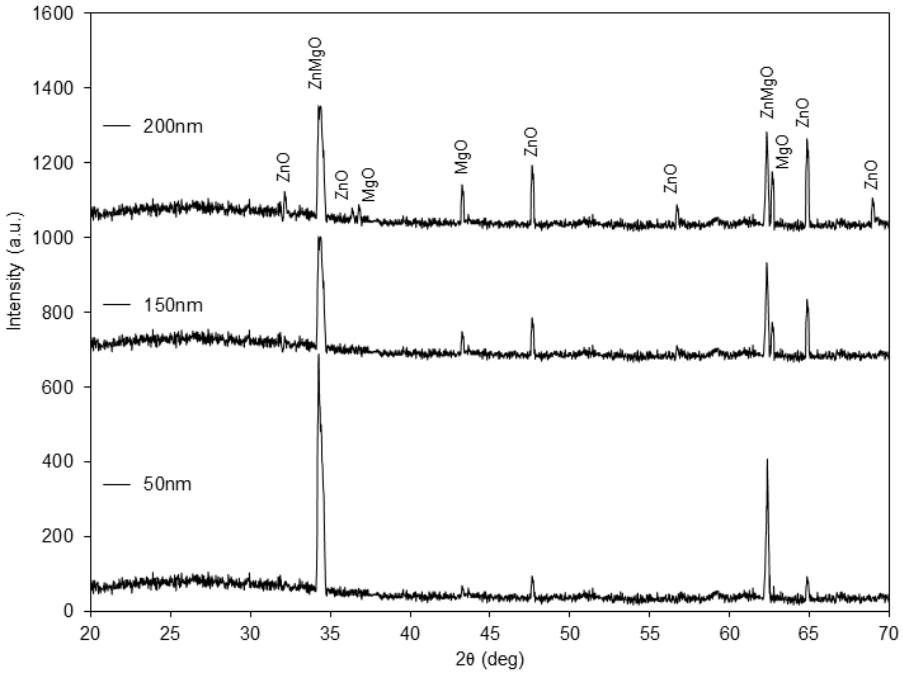

Fig. (3) The XRD patterns of the samples prepared from Mg targets coated with Zn films of different thickness (50, 150 and 200 nm)

The field-emission scanning electron microscope (FE-SEM) images in Fig. (4) offer a compelling visual comparison of ZnMgO samples prepared using two distinct laser energies. The image in Fig. (4a) displays a highly interconnected and seemingly denser arrangement of ZnMgO nanoparticles. The predominant morphology appears to be an aggregation of rod-like or elongated structures that are extensively entangled and form a porous, yet compact, network. There's a notable degree of uniformity in the size and shape of these individual structures, which appear to be in the nanometer to sub-micrometer range. The overall impression is one of a material with a high surface area due to the intricate interconnections, but also potentially exhibiting good structural integrity due to the robust linking of particles. This morphology could suggest a more efficient growth or deposition process where the laser energy facilitated the formation of these elongated structures and their subsequent aggregation into a cohesive mass. The tightly packed nature might lead to different optical, electrical, or catalytic properties compared to a more dispersed structure [40].

In contrast, the image in Fig. (4b) reveals a noticeably different morphology. Here, the ZnMgO particles appear more discrete and less interconnected. While elongated or rod-like structures are still present, they are more isolated and dispersed within a matrix that seems to consist of finer, possibly amorphous, background material or smaller unaggregated particles. There's a greater degree of separation between the individual larger structures, and they do not form the same extensive, interconnected network observed in the first image. The overall arrangement seems less dense and more open. This could indicate that the laser energy used for this sample resulted in less efficient

 ISSN (print) 2958-8960 (online) 3006-6042 Printed in IRAQ

aggregation or even promoted the growth of individual particles with less propensity to self-assemble into larger, intertwined structures. The presence of a finer background matrix could also suggest different growth kinetics, perhaps leading to the formation of smaller nanoparticles that don't coalesce as readily. The variation in particle distribution and the presence of more isolated structures could impact properties such as crystallinity, defect density, and ultimately the performance of the material in applications.

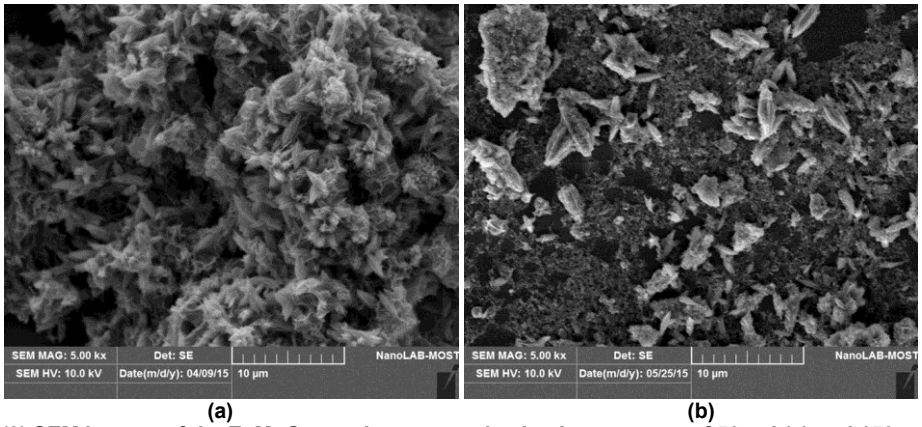

(a) (b)

Fig. (3) SEM images of the ZnMgO samples prepared using laser energy of 50 mJ (a) and 150 mJ (b)

Analyzing the scale bar, which represents 10 µm in both images, allows for an estimation of the size of the features. In both cases, the individual elongated structures appear to be in the range of a few micrometers in length, with widths in the sub-micrometer range. However, the arrangement and density of these features are the key differentiators. The first image showcases a microstructure dominated by large clusters of interconnected elongated particles, while the second image presents a more fragmented landscape with more spatially separated particles.

The differences in morphology between the two samples are likely attributable to the distinct laser energies employed during their preparation. Higher laser energy can influence various aspects of material synthesis, including deposition rate, particle nucleation and growth kinetics, and the degree of particle agglomeration. For instance, a higher laser energy might lead to more rapid material ablation and subsequent particle formation, potentially resulting in larger, more interconnected structures (as seen in the first image). Conversely, a different laser energy might promote the formation of smaller, more dispersed particles or inhibit strong inter-particle bonding (as suggested by the second image). These morphological variations directly impact the material's properties, including its surface area, porosity, mechanical stability, and ultimately its functional performance in devices or catalytic reactions. Understanding this correlation between laser energy and morphology is crucial for optimizing the synthesis parameters to tailor the properties of ZnMgO for specific applications.

4. Conclusions

The ZnMgO thin film analysis reveals a consistent deposition rate of 1.70 nm/min, crucial for reproducible properties. The Zn layer thickness dictates crystallinity, grain size, and phase formation. Optimal ZnMgO alloying occurs at 150 nm Zn thickness, while 50 nm shows limited alloying and 200 nm exhibits increased phase separation. The laser energy's impact on morphology is revealed as higher energy yields interconnected ZnMgO networks, whereas lower energy results in discrete particles. These findings underscore the importance of precise control over both sputtering time (Zn thickness) and laser energy to tailor ZnMgO thin film characteristics for various device applications.

References

[1] L. Trinkler et al., “Characterization of wurtzite Zn1−xMgxO epilayers grown on $ScAlMgO_4$ substrate by methods of optical spectroscopy”, J. Alloys Comp., 912 (2022) 165178.
[2] D. Kuang et al., “Dual-ultraviolet wavelength photodetector based on facile method fabrication of ZnO/ZnMgO core/shell nanorod arrays”, J. Alloys Comp., 860 (2021) 157917.
[3] N. Karthikeyan, A. John Peter, and C.W. Lee, “Induced electrostatic fields on optical gain in a polar quantum dot”, Chem. Phys. Lett., 760 (2020) 138021.
[4] Y. Li et al., “Investigation of properties of ZnO and MgxZn1-xO films prepared by sol-gel method”, J. Mol. Struct., 1261 (2022) 132959.
[5] F. Bellarmine et al., “Observation of ultraviolet whispering gallery modes in ZnMgO microrods”, J. Lumines., 210 (2019) 404-407.

[6] U.U. Rehman et al., "Wedge-shape Al and Mg co-doped zinc oxide thin films: A Facile Route to achieve high thermoelectric power factor", Ceram. Int., 50(19B) (2024) 36394-36401.
[7] M.A. Pietrzyk et al., "Self-organized ZnMgO nanocolumns with ZnO/ZnMgO quantum wells on c-plane Al_2O_3 substrates by MBE: Growth conditions and properties", J. Alloys Comp., 737 (2018) 748-751.
[8] P. Masiak, I. Gorczyca, and H. Teisseyre, "Theoretical study of the electronic and optical properties of ZnO/MgO rock salt superlattices", Micro Nanostruct., 182 (2023) 207647.
[9] R. Yousefi and M.R. Muhamad, "Effects of gold catalysts and thermal evaporation method modifications on the growth process of $Zn_{1-x}Mg_xO$ nanowires", J. Solid State Chem., 183(7) (2010) 1733-1739.
[10] A. Kaushal, and D. Kaur, "Pulsed laser deposition of transparent ZnO/MgO multilayers", J. Alloys Comp., 509(2) (2011) 200-205.
[11] L. Wang et al., "Highly transparent and thermal-stable silver nanowire conductive film covered with ZnMgO by atomic-layer-deposition", J. Phys. Chem. Solids, 111 (2017) 328-334.
[12] M. Caglar, Y. Caglar, and S. Ilican, "Investigation of the effect of Mg doping for improvements of optical and electrical properties", Physica B: Cond. Matter, 485 (2016) 6-13.
[13] A. Kazmierczak-Balata et al., "Microscopic study of local thermal, electrical and structural properties of ZnMgO thin films on different substrates", Micron, 195 (2025) 103837.
[14] F. Ercan et al., "Structural, optical, and electrical properties of $Zn_{(1-x)}Mg_xO$ nano-compounds and $ZnO/Zn_{(1-x)}Mg_xO$ heterostructures", Mater. Chem. Phys., 290 (2022) 126479.
[15] E. Zielony and M.A. Pietrzyk, "Diode characteristics of ZnO/ZnMgO nanowire p-n junctions grown on Si by molecular beam epitaxy", Mater. Sci. Eng. B, 268 (2021) 115148.
[16] K. Medjnoun et al., "Characteristics of nanostructured $Zn_{1-x}V_xO$ thin films with high vanadium content elaborated by rf-magnetron sputtering", Superlatt. Microstruct., 82 (2015) 384-398.
[17] F.Z. Aouacheria et al., "Experimental and theoretical study on structural and electronic properties of $Zn_{1-x}Mg_xO$ from (x=0 to 0.375) in wurtzite phase", Micro Nanostruct., 164 (2022) 107155.
[18] S.C. Su et al., "Oxygen flux influence on the morphological, structural and optical properties of $Zn_{1-x}Mg_xO$ thin films grown by plasma-assisted molecular beam epitaxy", Appl. Surf. Sci., 254(15) (2008) 4886-4890.
[19] C. Abed et al., "Growth, structural and optical properties of ZnO-ZnMgO-MgO nanocomposites and their photocatalytic activity under sunlight irradiation", Mater. Res. Bull., 110 (2019) 230-238.
[20] M. Xing et al., "Mg-doped ZnO layer to enhance electron transporting for PbS quantum dot solar cells", Curr. Appl. Phys., 21 (2021) 14-19.
[21] N. Guo et al., "Preparation and optical properties of Mg-doped ZnO nanorods", Appl. Surf. Sci., 317 (2014) 400-404.
[22] H. Ferhati et al., "Highly sensitive, ultra-low dark current, self-powered solar-blind ultraviolet photodetector based on ZnO thin-film with an engineered rear metallic layer", Mater. Sci. Semicond. Process., 110 (2020) 104957.
[23] T. Brouri et al., "Interplay effects of humidity and UV light sensitivities of $Zn_{0.9}Mg_{0.1}O$ nanogranular thin films", Appl. Surf. Sci., 353 (2015) 933-938.
[24] T.-W. Chiu et al., "$Zn_{1-x}Mg_xO$/ZnO heterostructures studied by Kelvin probe force microscopy conjunction with probe characterizer", Appl. Surf. Sci., 256(4) (2009) 1180-1183.
[25] H.C. Jeon et al., "Enhancement of optical gain in Li:CdZnO/ZnMgO quantum well lasers", Physica E: Low-dimen. Syst. Nanostruct., 42(10) (2010) 2652-2654.
[26] A. Rivera, A. Mazady, and M. Anwar, "Co-axial core–shell ZnMgO/ZnO NWs", Solid-State Electron., 104 (2015) 126-130.
[27] Z. Yin et al., "Enhanced performance of UV photodetector based on ZnO nanorod arrays via TiO_2 as electrons trap layer", Mater. Sci. Semicond. Process., 148 (2022) 106813.
[28] K. Belahlou et al., "Tuned band gap in green-synthesized ZnO, MgO, and $Zn_{1-x}Mg_xO$ for photocatalytic degradation of chlorophenylurea herbicide under UV-A and solar light in diverse water matrices", Separat. Purif. Technol., 376(3) (2025) 134038.
[29] M.A. Pietrzyk et al., "Properties of ZnO/ZnMgO nanostructures grown on r-plane Al_2O_3 substrates by molecular beam epitaxy", J. Alloys Comp., 650 (2015) 256-261.
[30] C. Gao et al., "Enhanced photovoltaic and piezo-photovoltaic effects in flexible oxide ferroelectric film directly coated on polyimide substrate", Nano Energy, 117 (2023) 108839.
[31] G. Gupta and S. Rath, "Microstructural investigations of green-synthesized wurtzite-phase ZnMgO nanopowders and their defect-mediated ferromagnetism", Mater. Res. Bull., 148 (2022) 111671.
[32] R.N. Gayen et al., "Zinc magnesium oxide nanofibers on glass substrate by solution growth technique", J. Cryst. Growth, 310(18) (2008) 4073-4080.
[33] A. Mazady, A. Rivera, and M. Anwar, "Optical parameters of $Zn_{1-x}Mg_xO$ nanowires in THz regime", Solid-State Electron., 101 (2014) 8-12.
[34] C.-J. Pan et al., "Structural and optical properties of ZnMgO nanostructures formed by Mg in-diffused ZnO nanowires", J. Solid State Chem., 180(4) (2007) 1188-1192.
[35] B.S. Kwak et al., "Synthesis of basalt fiber@$Zn_{1-x}Mg_xO$ core/shell nanostructures for selective photoreduction of CO_2 to CO", Appl. Surf. Sci., 407 (2017) 109-116.
[36] M.A. Pietrzyk et al., "Optical investigations of ZnO/ZnMgO quantum wells in self-assembled ZnMgO nanocolumns grown on Si (111) by MBE", J. Lumines., 179 (2016) 610-615.
[37] N.S. Minimala, A. John Peter, and C.W. Lee, "Electric field induced nonlinear optical properties of a confined exciton in a $ZnO/Zn_{1-x}Mg_xO$ strained quantum dot", Physica E: Low-dimen. Syst. Nanostruct., 48 (2013) 133-139.
[38] M.A. Pietrzyk et al., "Optoelectronic properties of ZnO/ZnMgO multiple quantum wells in ZnMgO nanocolumns grown on Si (111)", J. Alloys Comp., 717 (2017) 41-47.
[39] X. Cui et al., "Metal oxide charge transport layer targeting efficient and stable perovskite light-emitting diodes", J. Alloys Comp., 960 (2023) 170823.
[40] U.C. Matur, I.P. Duru, and D. Akcan, "Tracking optical properties of ZnO:Mg thin films: Experimental and first principles calculations", Ceram. Int., 48(13) (2022) 19090-19097.

 ISSN (print) 2958-8960 (online) 3006-6042 Printed in IRAQ